

## **Development and validation of pattern recognition algorithm and suppression pool flow modelling**

Patel Giteshkumar, Puustinen Markku, Hyvärinen Juhani, Hujala Elina, Tanskanen  
Vesa

This is a Author's accepted manuscript (AAM) version of a publication  
published by American Nuclear Society

in Proceedings of 20th International Topical Meeting on Nuclear Reactor Thermal Hydraulics,  
NURETH-20

**DOI:** 10.13182/NURETH20-40197

### **Copyright of the original publication:**

© American Nuclear Society

### **Please cite the publication as follows:**

Patel, G., Puustinen, M., Hyvärinen, J., Hujala, E., Tanskanen, V. (2023). Development and validation of pattern recognition algorithm and suppression pool flow modelling. Proceedings of the 20th International Topical Meeting on Nuclear Reactor Thermal Hydraulics (NURETH-20). 3285. pp. 808-821.

**This is a parallel published version of an original publication.  
This version can differ from the original published article.**

# Development and validation of pattern recognition algorithm and suppression pool flow modelling

**Giteshkumar Patel\*, Markku Puustinen, Juhani Hyvärinen**

<sup>a</sup> LUT University

Yliopistonkatu 34, 53850 Lappeenranta, Finland

giteshkumar.patel@lut.fi, markku.puustinen@lut.fi, juhani.hyvarinen@lut.fi

**Elina Hujala<sup>a,b</sup>**

<sup>b</sup>Université de Fribourg

CH-1700 Fribourg, Switzerland

elina.hujala@lut.fi

**Vesa Tanskanen**

Stressfield Oy

Laserkatu 6, 53850, Lappeenranta, Finland

vesa.tanskanen@stressfield.fi

## ABSTRACT

The comprehensive understanding of the dynamics of vapour bubbles and jets discharged from vent pipes and spargers into subcooled liquid has a significant role in assessing the capability of nuclear safety systems to perform their function properly. However, high-resolution local measurements and numerical calculations of these complex and rapidly condensing gas volumes are challenging due to rapid pressure oscillations, microscopic length, and time scales of turbulent two-phase flow. Visual observation of the interior of test section can make modern measurement techniques a viable alternative in such cases.

This paper presents the work concerning the modelling of vertical (vent) and horizontal (sparger) steam injection in a water pool by applying the Eulerian-Eulerian two-fluid approach. In this work, the formation and collapse of the steam bubbles in chugging condensation mode and bubbling condensation oscillation mode are evaluated by using pattern recognition (PR) algorithm. The PR algorithm is based on video material recorded during the direct contact condensation (DCC) experiments of PPOOLEX and SEF-POOL test facilities. The velocity of collapsing bubbles is estimated with the PR algorithm. The accuracy of PR algorithm is cross-checked with the CFD simulation results. Results indicate that the presented PR algorithms provide important information on the dynamics of phase interface in all directions. These details are advantageous for comprehensive DCC and steam-water surface instability model development. Results show that inclusion of interfacial instability modelling i.e., the Rayleigh-Taylor interfacial area model in Eulerian two-fluid simulation, inevitably improved the interface roughness and thereby heat transfer, which controls bubble growth and collapses.

## KEYWORDS

CFD, Pattern recognition, Interface, DCC, Chugging

## 1. INTRODUCTION

An understanding of the dynamics of the bubbles and jets discharged from vent pipes and spargers into a subcooled water pool and associated direct contact condensation (DCC) phenomena is vital from the thermal

---

\*Corresponding author

hydraulics and safety analysis point of view of the nuclear power plants. DCC is governed predominantly by the liquid side convection and conduction near the two-fluid interface. A steam injection causes heat, momentum, and mass sources and eventually develops thermal stratification or mixing in the pressure suppression pool. The development of thermal stratification in the pressure suppression pool (PSP) can be a safety hazard as it significantly obstructs the condensation capacity of injected steam which raises the pool surface temperature and containment pressures [1]. Further, momentum resulting from the steam blowdowns induces hydrodynamic loads to the pool structures and submerged venting systems. However, direct local and high-resolution measurement of steam blowdown tests is extremely demanding because of the pressure oscillation due to the rapid condensation and intricate and micro-scale two-phase flow phenomena of DCC. Although, if visual observation of the PSP interior is possible then modern measurement techniques like high-speed cameras could be a viable alternative. Recently, some researchers e.g. [2,3] have presented data analysis methods with a high-speed video recording of DCC. Current state-of-the-art two-phase computational fluid dynamics (CFD) codes allow practical modelling of steam DCC in a PSP. Several authors e.g. [4-9] have published their works concerning CFD simulations of DCC including large vents and spargers by employing different numerical approaches.

This paper presents the CFD simulations of the drywell-wetwell suppression pool system PPOOLEX and the small-scale separate effect test facility (SEF-POOL) experiments of Lappeenranta-Lahti University of Technology (LUT University). The simulations have been performed by using Eulerian-Eulerian two-fluid approach with NEPTUNE\_CFD and OpenFOAM CFD codes. The interfacial heat transfer between steam and water was modeled by using the Nusselt number formulation of Coste [10]. The Rayleigh-Taylor interfacial (RTI) area model of Pellegrini et al. [8] was applied for the interfacial area modeling. The formation and collapse of the steam bubbles in chugging condensation mode and bubbling condensation oscillation mode (BCO) are studied by using the pattern recognition (PR) algorithm.

## 2. SUPPRESSION POOL EXPERIMENTS AND METHODS OF ANALYSIS

Fig. 1(a) shows the schematic view of the PPOOLEX test facility of LUT University. The PPOOLEX test facility is a unique technical scale experimental facility for BWR containment safety-related research which consists of both the drywell and wetwell (condensation pool) compartments of the containment [11]. Several experiments have been performed with the PPOOLEX facility including thermal stratification and mixing experiments, steam condensation in the drywell compartment, and the effect of steam blowdown pipe outlet design and the number of blowdown pipes. The test facility is 7.45 m in height. The inner diameter is 2.4 m. The drywell compartment is thermally insulated to avoid wall condensation. The test events of the interior were recorded using high-speed video cameras through the installed windows on the side walls and in the bottom segment of the wetwell compartment.

DCC-05 experiment of PPOOLEX facility was aimed to acquire test data for the validation of DCC models used in CFD codes and to obtain the multi-camera high-speed video data of blowdown events to be used in the development work of PR algorithms. The DCC-05 blowdown test was subdivided into six different steam blows namely DCC-05-1 to DCC-05-6 according to steam mass flux. The average inlet steam mass flow rate in the test was  $0.1616 \text{ kg s}^{-1}$ . Further details about test conditions are discussed in Chapter 5. Test facility instrumentation consisted of three Phantom Miro M/R/ LC110 high-speed cameras. The recording framerate was 300 fps. Out of three cameras, one camera was recording at the bottom of the pool, under the blowdown pipe, and remaining two cameras were recording from the side of the pool, which was perpendicular to each other. More details about the instrumentation and data acquisition can be found in [12]. There were some challenges with the image quality of recorded tests. e.g., overexposed edges of the

bubbles due to lighting conditions. Also, transparent large bubbles were hard to recognize due to the swarms of tiny bubbles. Among all subtests, DCC-05-4 had the best quality video material and thus, it was selected in this work. Fig. 2(a) shows the recorded frames of the DCC-05-4 test. The different stages of steam bubble growth and collapse can be clearly seen. The red lines in the frames show the bubble boundaries recognized by the PR algorithm.

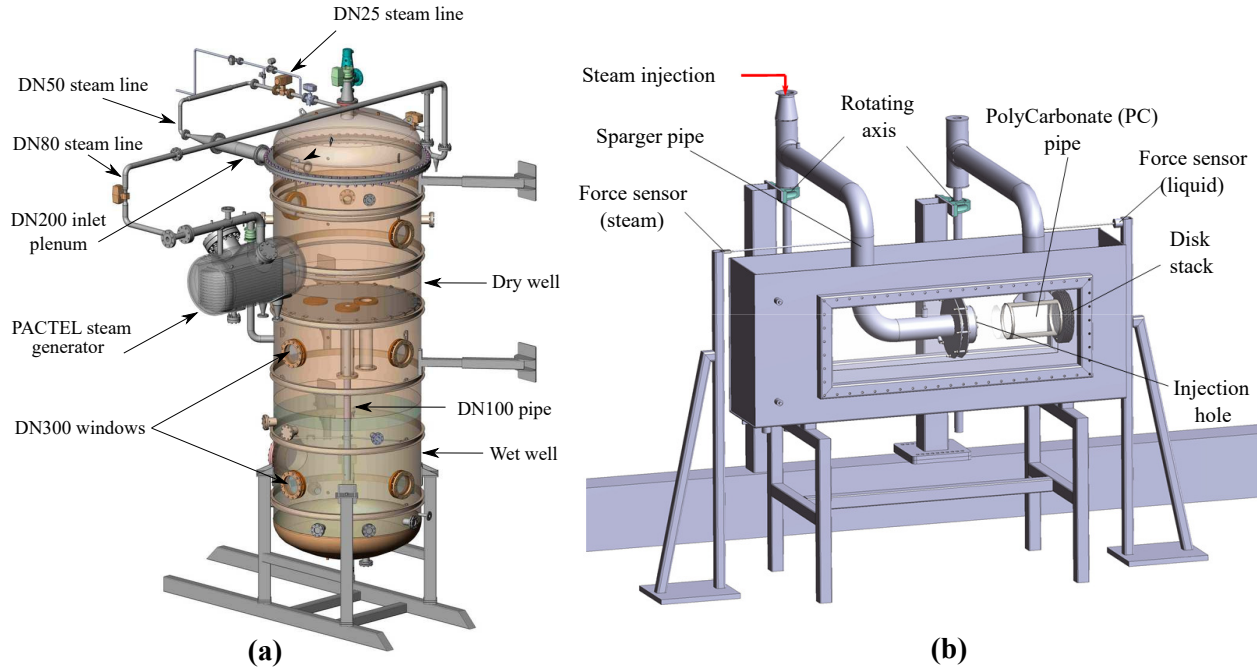


**Figure 1. (a) PPOOLEX and (b) SEF-POOL test facilities of LUT University.**

At LUT University, the SEF-POOL (Fig. 1(b)) was designed and constructed in cooperation with Kungliga Tekniska högskolan (KTH) for the Effective Heat and Momentum Source (EHS/EMS) model developments [13] and with Technical Research Centre of Finland (VTT) for the validation of EHS/EMS models with CFD simulations [14]. The phenomenological reference system for the SEF-POOL facility is the SRV sparger pipe of a BWR. The facility includes an open stainless steel rectangular box of 1.5 m long, 0.3 m wide, and 0.6 m high filled with water. Steam was injected to the pool horizontally through injection holes at the perforated plate at the end of the sparger pipe. The sparger pipe was thermally insulated. The installation of a polycarbonate (PC) pipe in the facility was aimed to generate a parallel flow pattern. The steam condenses in the PC pipe attached to the flow plate system which guides replacement water to the PC pipe. The PC pipe was 0.4 m long. The inner diameter of the PC pipe was about 0.144 m. In both test facilities, the steam generators of the Parallel Channel Test Loop facility were used as a steam source during the tests.

An extensive test series was performed with the SEF-POOL test facility to acquire test data on the characteristics of small-scale phenomena. From them, the SEF-INF2 experiment of the SEF-POOL test series was selected as the reference case for the PR algorithm development study and CFD simulations. The SEF-INF2 experiment was carried out with pool water temperatures varying from  $T_w = 317 \text{ K}$  to  $358 \text{ K}$ . The SEF-INF2 experiment had a total of six recorded clips named SEF-INF2-1...SEF-INF2-6 according to pool water temperature. In this work, the SEF-INF2-6 was selected as the reference case. According to the condensation regime map of Song et al. [15], this test was operated mainly in the BCO. The steam was injected by a single orifice with a diameter of 16 mm. During the test, the steam mass flow rate was kept constant at about

$36 \text{ g s}^{-1}$ . In the SEF-INF2-6 experiment, steam injection in the pool was recorded using high-speed video cameras with  $1024 \times 528$  pixel resolution at a frame rate of 2800 frames per second. Fig. 2(b) shows the bubble formation and detachment in the SEF-INF2-6 test. The clear continuous interface of the bubbles was visible in recorded frames. In the test, a steam plume started to grow at the orifice in the beginning. Unlike in the vertical steam blowdown test of the PPOOLEX, the steam bubbles expanded rapidly and detached from the sparger orifice. Following, they travelled forward oscillating and finally condensed in the pool water before leaving the PC tube.

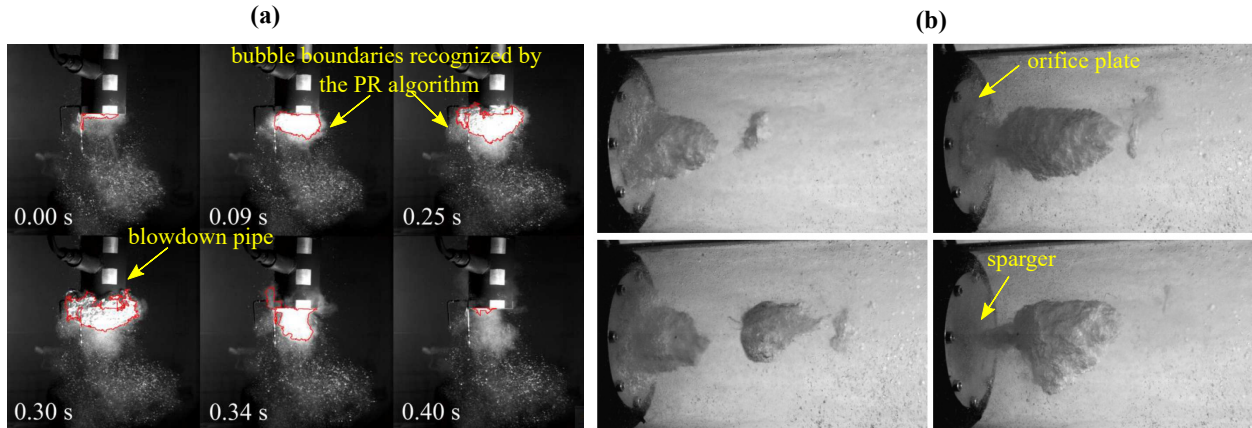


**Figure 2. Bubble formation and condensation during (a) the DCC-05-4 test of PPOOLEX and (b) the SEF-INF2-6 test of SEF-POOL.**

## 2.1. Pattern recognition algorithm for DCC-05 and SEF-INF2 experiments

The details of certain properties e.g. bubble surface velocity of the rapidly condensing steam injection cases can be important in reckoning turbulent properties at the interface, the size of the largest turbulent eddies which control the liquid-side heat transfer away from the interface, and thereby, the rate of condensation. However, the direct measurement of these parameters remains challenging even with modern instrumentation. In this work, the PR algorithm was used to acquire non-intrusive measurement data of intricate and rapidly condensing flow. The PR algorithm works in three segments: (1) pre-processing (all image processing is conducted in it), (2) simplified pattern recognition (identification of steam bubbles edges) and (3) post-processing (all image analysis and data assembly). The image analysis part was conducted by using MATLAB packages. For horizontal cases, pre-processing and edge detection of the bubble boundaries were based on the PR algorithm used for the vertical steam injection tests. The bubbles travel through the whole image, and the threshold values of the pixels vary largely. Thus, the image was divided into parts which can be separately modified by brightening and sharpening. The recorded frames were allotted into twenty parts. The best threshold value was found for the individual part and the grayscale image was converted to a binary image. Following the conversion process in the PR part, the edge of the bubbles was detected from the binary images by implementing the Moore neighbourhood algorithm modified by Jacob's stopping criteria. For recognizing the bubble parts from the frame, the image was compared with an empty background image (without a bubble). Thereby, the output image should comprise only the changed pixel values. More details about the PR algorithm can be found in [16]. Originally the PR algorithm was developed for the estimation of the volume and surface area of the condensing bubbles in vertical blowdown pipes. Also, surface velocity and acceleration were evaluated in the vertical direction using the so-called box ratio method [17, 18]. In the extended algorithm presented by Hujala et al. [17], multiple horizontally moving bubbles were tracked

and velocity as well as acceleration evaluation was improved to cover all angles from 0 to 360 degrees. In this paper, the extended algorithm was applied to the vertical blowdown pipe case of PPOOLEX and the horizontal sparger case of SEF-POOL. The bubble surface velocities  $\mathbf{v}_n$  were calculated for integer angles for all the recognized bubble interfaces in the tests and simulated cases. The velocities were evaluated relative to the center point of the blowdown pipes outlet for the PPOOLEX case. The distance between this center point and the recognized bubble surface was evaluated and the change in the distance was calculated using the forward difference method for obtaining the surface velocities. The same method was used to the CFD results for the estimation of bubble surface velocities. The bubble surface velocities were evaluated by using Eq. 1 [17].

$$\mathbf{v}_n = \begin{cases} F_S(-y_{n+1} - (-y_n)), & \text{when } n = 1 \\ \frac{F_S}{2}(-y_{n+1} - (-y_{n-1})), & \text{when } 2 \leq n \leq N. \end{cases} \quad (1)$$

Here  $y$  is the distance from the center of the bubble to the edge of the bubble, and  $n$  is the image of interest at frame rate  $F_S$ . While  $N$  indicates the total number of images in the recorded video of the experiment and the CFD simulations. Further details about the extended PR algorithm applied to the more complicated SEF-POOL test and simulations can be found in [19].

### 3. NUMERICAL MODELS

In this study, simulations of the steam injection tests were performed with the NEPTUNE\_CFD [20–22] and OpenFOAM CFD codes. For this purpose, compressible two-phase solver was used in which the steam-water system was simulated with the Eulerian-Eulerian two-fluid approach. In a two-fluid solver, mass, momentum, and energy equations can be written as below, respectively:

$$\frac{\partial}{\partial t} (\alpha_\phi \rho_\phi) + \nabla \cdot (\alpha_\phi \rho_\phi \mathbf{U}_\phi) = \Gamma_\phi, \quad (2)$$

$$\begin{aligned} \frac{\partial}{\partial t} (\alpha_\phi \rho_\phi \mathbf{U}_\phi) + \nabla \cdot (\alpha_\phi \rho_\phi \mathbf{U}_\phi \mathbf{U}_\phi) &= \alpha_\phi \nabla \cdot (\tau_{\phi,ij} + \tau_{\phi,ij}^t) \\ &\quad - \alpha_\phi \nabla P + \alpha_\phi \rho_\phi \mathbf{g} + \mathbf{M}_\phi + \alpha_\phi \mathbf{S}_\phi, \end{aligned} \quad (3)$$

$$\begin{aligned} \frac{\partial}{\partial t} (\alpha_\phi \rho_\phi H_\phi) + \nabla \cdot (\alpha_\phi \rho_\phi \mathbf{U}_\phi H_\phi) &= \alpha_\phi \frac{\partial P}{\partial t} + \alpha_\phi \rho_\phi \mathbf{U}_\phi \mathbf{g} \\ &\quad - \nabla \cdot (\alpha_\phi \mathbf{Q}_\phi) + \Gamma_\phi H_\phi + \Pi_\phi + q''_{\text{wall},\phi}. \end{aligned} \quad (4)$$

Here,  $\phi$  stands for an arbitrary phase.  $\alpha$  represents the volume fraction.  $\rho$  is the density and  $\mathbf{U}$  is the velocity. The mass source/sink per unit volume is indicated by  $\Gamma$ . In the momentum equation,  $\tau_{\phi,ij}$  and  $\tau_{\phi,ij}^t$  stand for the molecular and turbulent stress tensors, respectively.  $\mathbf{g}$  represents the gravitational force term.  $\nabla P$  indicates the overall pressure gradient.  $\mathbf{M}_\phi$  indicates the interfacial momentum transfer between phases which consists of all interfacial forces, e.g. drag, lift, virtual mass and wall lubrication. In this study, only the effect of drag force was considered by using the correlation of Schiller and Naumann [23]. However, in this rapidly condensing horizontal steam injection case, the condensation mass flow rate was high, and thus the possible minor effects of other interfacial forces were omitted from the simulations.  $\mathbf{S}$  indicates the external momentum source term. In the energy transport equation,  $H$  represents the total enthalpy.  $\mathbf{Q}$  and  $\Pi$  indicate the conductive heat flux and the bulk interfacial heat transfer rate, respectively.  $q''$  expresses a separate wall boiling/condensation heat source term.

In this work, the phase change model was used to simulate the DCC phenomena, which describes the phase change instigated by interphase heat transfer of adjacent convective flows. This approach is suitable only for phase change without non-condensables and covers the heat transfer processes on each side of the phase interface. By imposing the overall heat balance, the mass transfer due to the phase change at the steam-liquid interface was calculated as  $\Gamma_\phi = \frac{\Pi_1 + \Pi_2}{H_2 - H_1}$  where 1 stands for water and 2 for steam. In this work, the steam was in a saturated state, therefore in all the simulations, the vapour phase heat transfer contribution was negligible. The interfacial heat transfer for water was calculated by

$$\Pi_1 = a_i h_{HTC,1} (T_{\text{sat}} - T_1), \quad (5)$$

where  $h_{HTC,1}$  is the heat transfer coefficient for the water which can be written as follows:

$$h_{HTC,1} = \frac{\text{Nu}_1 \lambda_1}{L_1}. \quad (6)$$

Here,  $\lambda$  is the thermal conductivity and  $L$  is the length scale.  $\text{Nu}$  is the Nusselt number. Several correlations for the Nusselt number are available which can be applicable for DCC modeling of suppression pools. However, the previous works on DCC modeling of suppression pools have demonstrated that the Nusselt number correlations predicting high condensation rates in separated flow as Eulerian two-fluid cases are the most suitable. In this work, the continuous model of Coste [10] which provided high enough heat transfer rates for a rapid condensation was employed, and it can be written as follows,

$$\text{Nu}_1 = \text{Re}_{T,1}^{7/8} \text{Pr}_1^{1/2}, \quad (7)$$

where  $\text{Pr}$  is the Prandtl number and  $\text{Re}_{T,1}$  is turbulent Reynolds number ( $\text{Re}_{T,1} = \frac{V_{T,1} L_{T,1}}{\nu_1}$ ). The turbulent velocity and length scales:  $V_{T,1}$  and  $L_{T,1}$  in the  $\text{Re}_{T,1}$  are

$$V_{T,1} = \left(\frac{2}{3}k\right)^{1/2} \quad \text{and} \quad L_{T,1} = \left(\frac{\nu^3}{\varepsilon}\right)^{1/4}. \quad (8)$$

In Eq. (5),  $a_i$  is the interfacial area density. Capturing accurate interface behaviour is necessary for two-phase flow modeling when heat and mass transfer are involved in it. Various approaches can be used for obtaining interfacial area details based on the flow regime. In the separated flow cases where the interface is larger, smooth enough, and covers more than one computational cell, the interfacial area density can be calculated from the gradient of the volume fraction. However, the accuracy of interfacial area depends on the grid resolution in the computational domain firmly. In fact, the gradient of the volume fraction excludes the interface alterations which can be smaller in scale than the computational cells. During steam discharge into a subcooled water pool, pressure decrease within the vapor phase may induce interfacial accelerations which could be higher than the acceleration of gravity [8, 9] and these intense interfacial accelerations trigger interfacial instabilities (i.e., Rayleigh-Taylor instability [8, 24, 25]) which enlarge the two-phase interfacial roughness significantly. In this work, a simple Rayleigh-Taylor Interfacial (RTI) model proposed by Pellegrini et al. [8] was used to simulate the effect of the increased interfacial area. The RTI model employs the pressure gradient causing a force accelerating the gas-liquid interface. The interfacial area density can be expressed as

$$a_i = \left(\frac{\kappa_\lambda \eta}{\pi} + 1\right)^2 |\nabla \alpha_1|, \quad (9)$$

where  $\kappa_\lambda$  is the wave number and  $\eta$  is the interfacial wave amplitude. More details about the RTI model and its performance against the dense grid are presented in [9]. Flow turbulence was solved by employing the standard  $k - \varepsilon$  turbulence model which solves balance equations for the turbulence kinetic energy and the turbulence kinetic energy dissipation rate.

## 4. GEOMETRICAL DETAILS AND GRID GENERATION

Fig. 3 shows the schematic of 3D CFD domains and fully hexahedral computational grids of the PPOOLEX and SEF-POOL facilities. In the computational domains of PPOOLEX, the blowdown pipe was moved to the center axis of the vessel. Also, the inlet plenum was relocated to the top of the drywell. These changes have negligible effects on the wetwell phenomena due to the large size of the wetwell and relatively low inlet steam velocity. The gas space of the wetwell was included in the 2D-axisymmetric simulations but excluded from the 3D simulations. The 2D-axisymmetric geometry contained a  $1^\circ$  sector of the PPOOLEX pool. The grid density should be good enough in the rapid condensation simulations for computation of the gradient of the volume fraction in order to represent the bubble interface well. Both in 2D and 3D computational domains, the grid was refined inside the blowdown pipe and around the pipe tip region with a  $5 \times 5$  mm cell size. The 2D-axisymmetric and 3D domains contained 72000 and 525500 hexahedral computational cells, respectively. This grid was suitable for the standard wall functions approach ( $y^+ \approx 100$ ). The idea of coarse grid is to make transient simulations quick and let the RTI model to deal with the interfacial area prediction.

In the SEF-POOL test, water can enter into the PC pipe from the pool through the flange connecting the steam line to the PC pipe due to momentum transfer and pool mixing by steam injection. Thus, the CFD model of the SEF-POOL included the flange and pool area around the PC pipe (Fig. 3). In the 3D computational domain, only the horizontal section of the steam line in the pool was considered. The domain contains 318000 hexahedral computational cells. The grid was refined inside the PC pipe uniformly with a  $2.6 \times 2.65$  mm cell size. However, the first cell thickness in the PC pipe grid was kept according to the standard wall functions approach requirements.

## 5. SIMULATION SET-UP

In DCC-05-4 test simulations, the steam/water interface was initialized at the elevation of 1.8 m corresponding to the water level in the pool inside the blowdown pipe. All the walls of the domain were set to the adiabatic conditions. A no-slip boundary condition was applied to all the wall surfaces. The wall condensation was not included in the simulations. Thus, the portion of wall condensation was approximated by using the correlation of Chen et al. [26] and the amount of wall condensate was subtracted from the inlet steam mass flow rate. The reduced inlet steam mass flow rate was  $0.1399 \text{ kg s}^{-1}$  in the simulations. The initial drywell and wetwell pressures were set to 301310 Pa and 293370 Pa, respectively. The wetwell liquid temperature was initialized from 300.7 K to 315.6 K corresponding to the measured stratified conditions. Also, the temperature of the liquid plug in the blowdown pipe was initialized as stratified from 374.3 K to 405.6 K. Inlet steam temperature was set to 429.2 K.

In the SEF-INF-2-6 simulations, the pool water was stagnant and initialized with the hydrostatic pressure at 353.5 K temperature. A pressure inlet boundary condition was used at the steam inlet. The outlet boundary patch of the domain was set to atmospheric pressure (101325 Pa). The pool walls were considered to be adiabatic and no-slip boundary conditions were imposed on all the wall surfaces. The simulations of the SEF-POOL test were carried out by using the standard wall function on the wall surfaces. In all the OpenFOAM simulation cases, the steam was modeled as condensing ideal gas due to a lack of steam table availability. The saturation temperature was a function of pressure, which was estimated from the NIST Chemistry WebBook [27]. While in NEPTUNE\_CFD simulations, the steam tables of CATHARE code [22] were used. Simulations were performed with the adaptive time stepping (with the limit of  $\max \Delta t = 10^{-5}/10^{-6}$  s and  $\max \text{ CFL (Courant-Friedrichs-Lewy condition)} \leq 1$  or less).

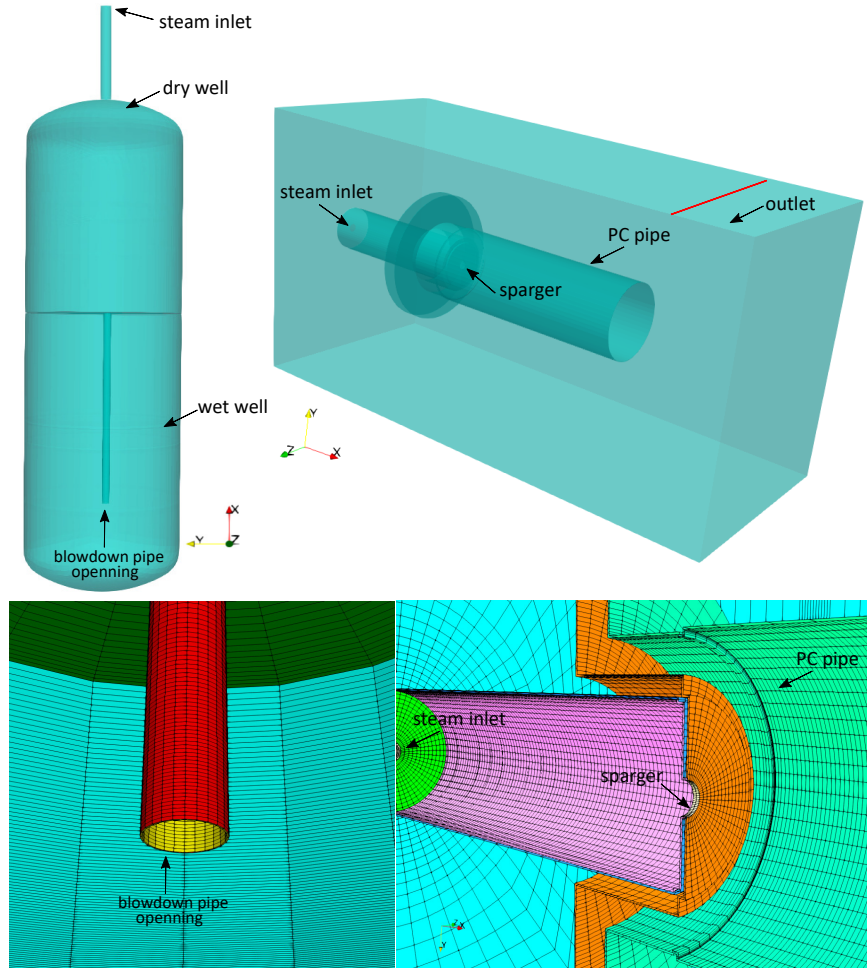
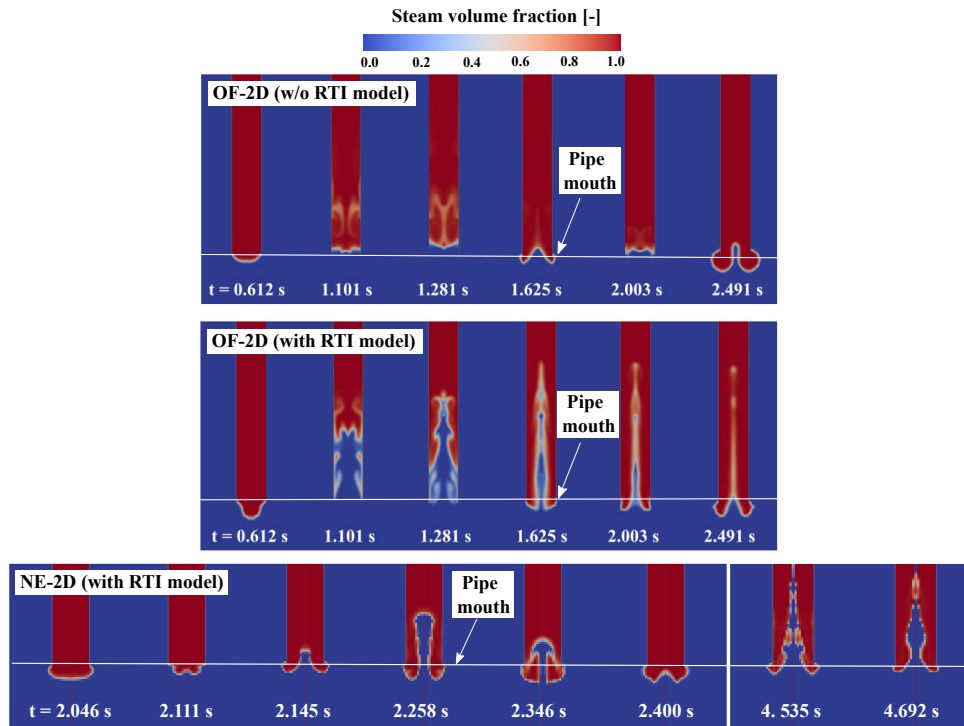


**Figure 3. CFD domains and computational grids of PPOOLEX and SEF-POOL test facilities.**

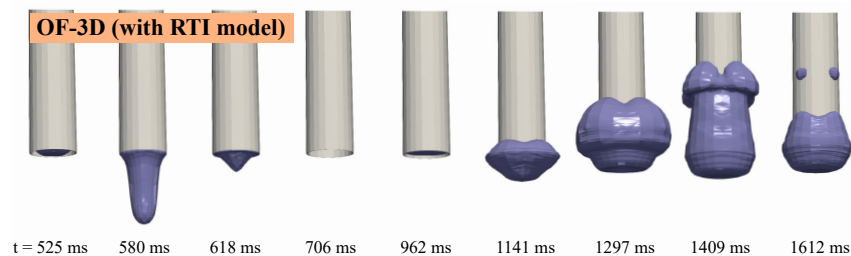
## 6. RESULTS AND DISCUSSION

In this work, both 2D-axisymmetric and 3D simulations of PPOOLEX DCC-05-4 were performed. However, the adaptive time stepping of OpenFOAM led to a very small time step size which had a significant influence on the simulation progress. Thus, the simulated transient of 3D cases was short. Fig. 4 compares the volume fraction fields of steam in the 2D-axisymmetric OpenFOAM and NEPTUNE\_CFD simulations of the DCC-05-4 test of PPOOLEX. The results of the OpenFOAM case without the RTI model are shown too. It was found out that chugging may vanish or stay too weak qualitatively despite high Nu numbers provided by DCC correlations. Pellegrini et al. [8] and Patel et al. [9] showed that the RTI model is necessary to increase the condensation rate properly to reach qualitatively correct chugging. In the beginning at  $t=0$  s, the steam/water interface was inside the blowdown pipe. As the steam mass flux increased, the interface moved downwards inside the blowdown pipe and a steam bubble formed at the pipe outlet. Results show that injected steam formed bubbles which condensed promptly. It was observed that a highly turbulent trail was generated when the pool water was pushed towards the bottom of the pool by steam during the initial blowdown. As time elapsed, the turbulence kinetic energy was enhanced further around the blowdown pipe and pool bottom. Accordingly, the turbulent mixing processes maintained the turbulence level in the pool water sustaining a certain DCC rate to provoke chugging motion [6]. In the case with the RTI model, after

the initial steam bubbles collapsed, the steam/water interface retreated further inside the blowdown pipe than in the case of excluding the RTI model. 2D simulations with OpenFOAM and NEPTUNE\_CFD predicted at best just weak chugging without the RTI model. After including the RTI model, chugging got qualitatively more aggressive, having a higher frequency and smaller bubble size. It was not possible to get chugging in a 3D model without the RTI model. By enabling the RTI model, also chugging started (Fig. 5).



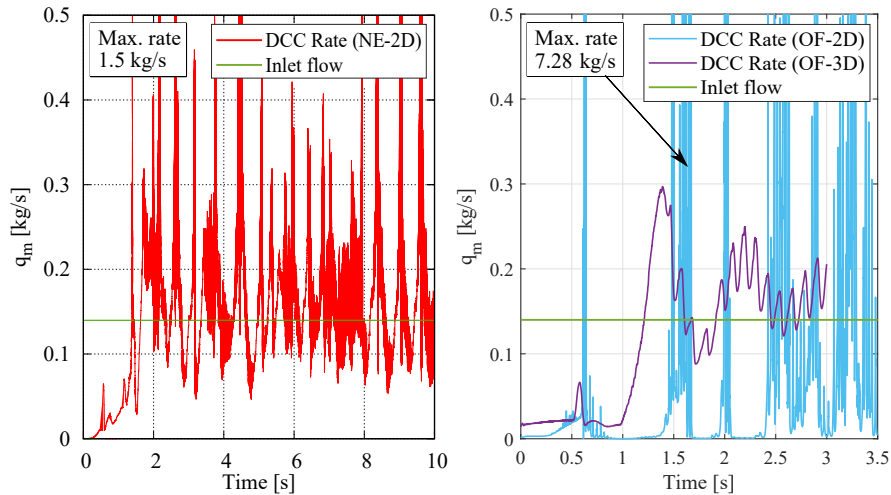
**Figure 4. Volume fraction fields of steam in the 2D-axisymmetric OpenFOAM and NEPTUNE\_CFD simulation of the PPOOLEX DCC-05-4 experiment.**



**Figure 5. Volume fraction fields of steam in the 3D OpenFOAM simulation of the PPOOLEX DCC-05-4 experiment.**

Persistent chugging requires that DCC mass flow rate increases much above the steam inlet rate, but also decreases below it. These occur in all the simulations with the RTI presented here (Fig. 6). The condensation rate is much higher in the OpenFOAM 2D simulations (max  $7.28 \text{ kg s}^{-1}$ ) than in the corresponding NEPTUNE\_CFD 2D simulation (max  $1.5 \text{ kg s}^{-1}$ ). Nevertheless, the DCC rates are likely too high in 2D simulations because all the local high condensation rate cells represent a high condensation rate ring in 3D

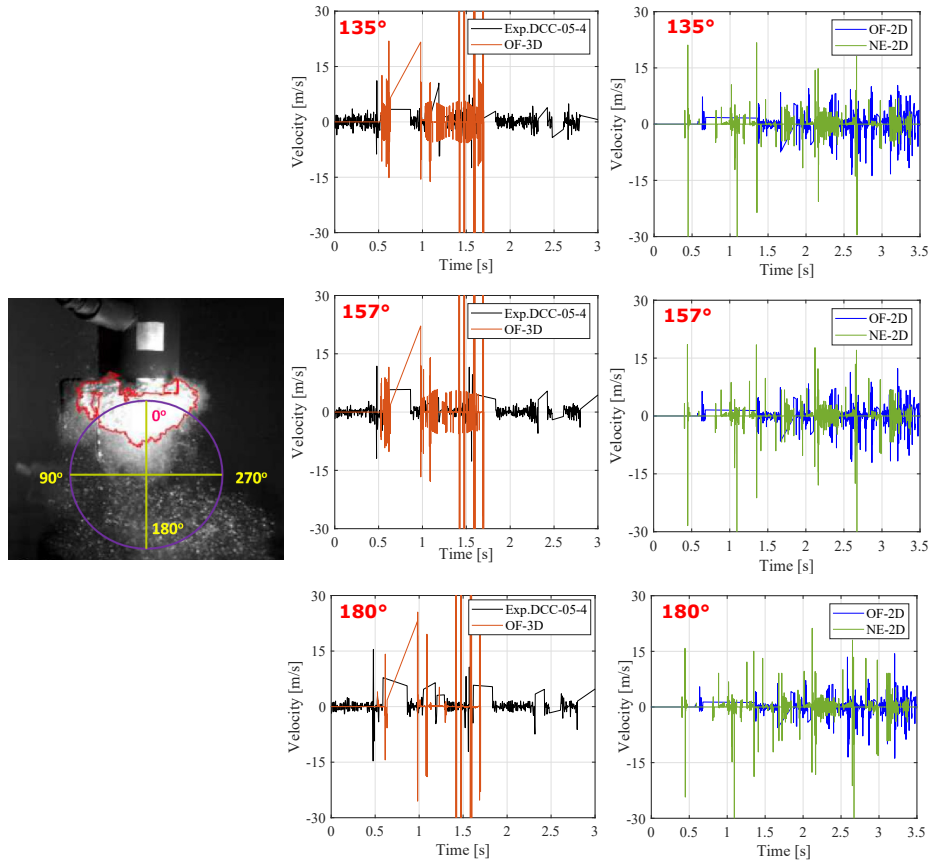
space. Also, the low condensation rate cells represent a ring in 3D space, but they at least have a minimum limit for the condensation rate, which is zero. Results show that the DCC rates in the 3D simulations were milder than in the 2D simulations.



**Figure 6. Condensation mass flow rate in the NEPTUNE\_CFD and OpenFOAM simulations of the PPOOLEX DCC-05-4 experiment.**

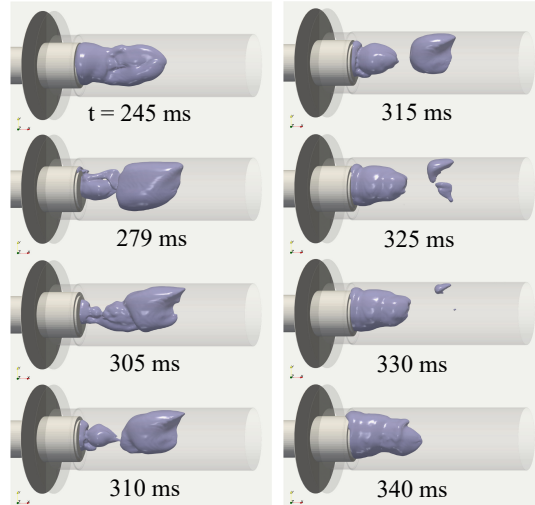
Fig. 7 compares the calculated bubble surface velocities at different angles in the DCC-05-4 experiment with the simulated cases. In the vertical vent pipe case, the bubbles hardly ever detached from the mouth of the blowdown pipe. Thus, most of the bubbles were just like “half-spheres”. Here, 0° direction faced towards the center of the blowdown pipe mouth and 180° direction indicated the bubble front (towards the pool bottom) as the angle increased counterclockwise. However, there were some challenges with the DCC-05-4 test video material. There were multiple disturbing objects and swarms of small bubbles which were interfering with the recognition process. Almost half of the bubble was always lost due to shadows. Thus, bubble surface recognition in the test was limited to approximately 130° to 230° (i.e.  $\pm 50^\circ$  around window axis). In the test, the largest bubble surface reached up to 0.15 m below the blowdown pipe mouth during expansion with a velocity of  $-15 \text{ m s}^{-1}$  and then condensed with an almost similar speed in the straight upward vertical direction. In NEPTUNE\_CFD simulations, the bubble surface velocity reached up to  $30 \text{ m s}^{-1}$  while condensing. The bubble surface velocity changes are comparable between OpenFOAM and NEPTUNE\_CFD cases at different angles. However, in 3D simulations, the highest velocity reached up to  $\pm 40 \text{ m s}^{-1}$  at some instances. The 1000 fps frame rate of the CFD simulations was suitable but the DCC-05-4 video material was recorded with a low 300 fps frame rate, which was noticed to be too low in most cases. Therefore, there might be some rapid motion of the bubble surface often, condensing surface oscillates before collapse which cannot be seen because of this low frame rate.

Figure 8 displays the instantaneous volume fraction fields showing the formation and condensation of bubbles in the 3D OpenFOAM simulation of the SEF-INF2-6 experiment. Results indicate that a steam plume started to grow at the orifice at the beginning of each bubble cycle, following its growth in the PC pipe. The pressure gradient inside the steam bubble is lesser than the surrounding water which invokes interfacial accelerations. Interfacial accelerations prompt interfacial instabilities and instigate roughening of the phase interface leading to condensation. Simulations captured all the phases of bubble lifetime, i.e. bubble expansion near the orifice, its detachment from the orifice and the end of its lifetime due to rapid condensation.



**Figure 7. The bubble surface velocities in different directions of a tracked bubble in the PPOOLEX DCC05-4 experiment and the simulated case.**

The formation and condensation of the bubbles in the simulations corresponded well with the test (Fig. 2 (b)). The estimated bubble surface velocities at different angles throughout the life span of the recognized bubble in the SEF-INF2-6 experiment and the simulated cases are compared in Fig. 9. The bubble surface velocity was calculated for all integer angles from  $0^\circ$  to  $360^\circ$  for all recognized bubbles. The bubble surface velocities were evaluated using center of mass and the forward-difference method (Eq. 1) with a resolution of  $1^\circ$ . Here,  $0^\circ$  faced towards the orifice and  $180^\circ$  direction referred to the bubble front as the angle increased counterclockwise. The positive velocity values denote the bubble growth direction. During the entire bubble life span, notable changes were observed in the surface velocity. Both in the test and the simulated cases, more activity was visible in the upward directions  $250^\circ$  to  $300^\circ$ , while in the downward direction, surface velocity remained relatively low. The largest velocities were identified near  $45 \text{ ms}^{-1}$ . While in the rearward directions of the bubble, the velocity remained smaller during the whole lifetime of the bubble. Gravity does not have much effect on that direction, so roughening to invoke condensation does not start there as easily as e.g. on the upper interface direction. At some angles, CFD simulations missed high peaks of velocities. Otherwise, surface velocity scales in the CFD simulations corresponded well to the SEF-INF2-6 test results defined with the help of the PR algorithm.



**Figure 8. Volume fraction fields of steam in the 3D OpenFOAM simulation of the SEF-POOL SEF-INF2-6 experiment.**

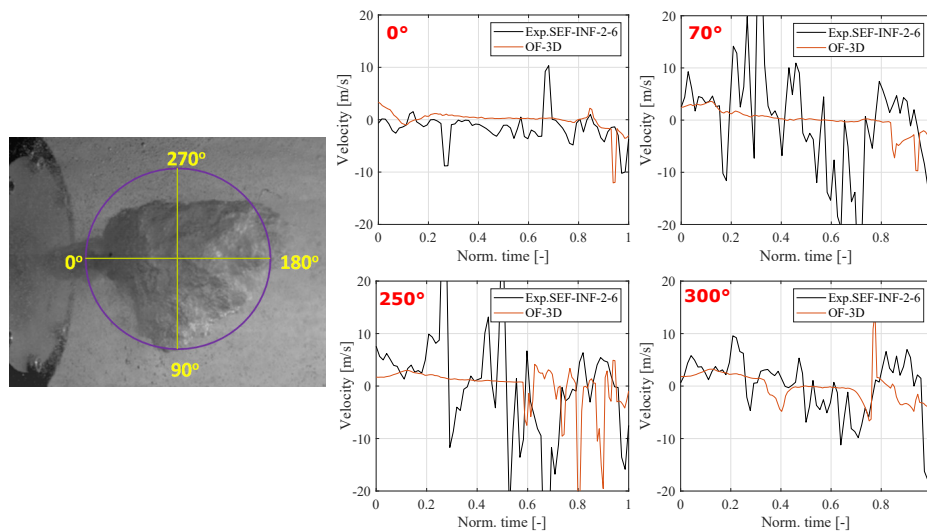


**Figure 9. The bubble surface velocities in different directions of a tracked bubble in the SEF-POOL SEF-INF2-6 experiment and the simulated case.**

## 7. CONCLUSIONS

This paper presents the work concerning the modelling of steam injection in a water pool by applying the Eulerian-Eulerian two-fluid approach with NEPTUNE\_CFD and OpenFOAM CFD codes. A pattern recognition-based image analysis (PR) algorithm was designed and developed further in this study. The direct contact condensation (DCC) experiment of the PPOOLEX and the SEF-POOL test facilities were used as the reference tests. The high-speed camera recordings of the tests were used to track rapidly condensing bubbles. The PR algorithm performed well with both the chugging and bubbling condensation oscillation modes of rapidly condensing steam bubbles. It recognized and tracked steam/water interfaces successfully throughout their entire life span. The presented PR algorithms provided important information on the dynamics of the phase interface. This study shows that the presented PR algorithm can be useful for the design

of improved thermal hydraulics test set-ups and can extract important data on intricate flow phenomena which is useful for the validation of the DCC models for different CFD codes.

Results emphasize that a high DCC heat transfer rate causes strong suction and reshaping of the steam/water interface. The large and rapid accelerations prompt interfacial instability. Thus, the interfacial area obtained from only the gradient of the volume fraction is not sufficient for provoking high DCC rates if the interface is rough, and its details tend to smear into the subgrid scale for a coarser grid. Results show that the inclusion of modelling of interfacial instabilities enhanced the interface roughness and DCC rates. This work shows that the continuous model of Coste [10] with the RTI model of Pellegrini et al. [8] improved condensation rates and predicted well both the cases of vertical (vent) and horizontal (sparger) steam injection in a water pool. The calculated surface velocity scales of the CFD simulations corresponded well with the test results. It is likely that further validation of DCC models should be carried out in 3D CFD-simulations.

## ACKNOWLEDGMENTS

The research leading to these results is funded by the Finnish Nuclear Waste Management Fund (VYR) via The Finnish Research Program on Nuclear Power Plant Safety SAFIR2022. The authors gratefully acknowledge this support.

## REFERENCES

1. H. Li, W. Villanueva, and P. Kudinov, "Effective Momentum and Heat Flux Models for Simulation of Stratification and Mixing in a Large Pool of Water," Nks report nks-266, NKS, Nordic nuclear safety research (2012), ISBN 978-87-7893-339-3.
2. S. Al Issa, P. Weisensee, and R. Macián-Juan, "Experimental investigation of steam bubble condensation in vertical large diameter geometry under atmospheric pressure and different flow conditions," *International Journal of Heat and Mass Transfer*, **70**, pp. 918–929 (2014).
3. K. Lee, "Experimental investigation on steam-water direct contact condensation using laser-induced fluorescence (LIF)," Master thesis, Texas A&M University, Department of Nuclear Engineering, 2019.
4. M. Meier, *Numerical and experimental study of large steam-air bubbles injected in a water pool*, PhD thesis, ETH, Swiss Federal Institute of Technology, Zurich, 1999, DISS. ETH No. 13091.
5. T. Pättikangas, J. Niemi, J. Laine, M. Puustinen, and H. Purhonen, "CFD modelling of condensation of vapour in the pressurized PPOOLEX facility," *Proc. CFD for Nuclear Reactor Safety Applications (CFD4NRS-3) Workshop, Bethesda, MD, USA, 14-16 September 2010*, pp. 12 (2010).
6. V. Tanskanen, A. Jorden, M. Puustinen, and R. Kyrki-Rajamäki, "CFD simulation and pattern recognition analysis of the chugging condensation regime," *Annals of Nuclear Energy*, **66**, pp. 133–143 (2014).
7. S. K. Dahikar, M. J. Sathe, and J. B. Joshi, "Investigation of flow and temperature patterns in direct contact condensation using PIV, PLIF and CFD," *Chemical Engineering Science*, **65** (16), pp. 4606–4620 (2010).
8. M. Pellegrini, M. Naitoh, C. Josey, and E. Baglietto, "Modeling of Rayleigh-Taylor Instability for Steam Direct Contact Condensation," *Proc. The 16th International Topical Meeting on Nuclear Reactor Thermal Hydraulics (NURETH-16), Chicago, IL, August 30-September 4*, pp. 15 (2015).
9. G. Patel, V. Tanskanen, E. Hujala, and J. Hyvärinen, "Direct contact condensation modeling in pressure suppression pool system," *Nuclear Engineering and Design*, **321**, pp. 328–342 (2017).

10. P. Coste, "Computational Simulation of Multi-D Liquid-Vapor Thermal Shock with Condensation," *Proc. Proceedings of ICMF'04, Yokohama, Japan, May 30 - June 4*, (2004).
11. M. Puustinen, H. Partanen, A. Räsänen, and H. Purhonen, "PPOOLEX Facility Description," Technical report, Lappeenranta University of Technology (2006).
12. M. Puustinen, J. Laine, A. Räsänen, and A. Hujala, "Chugging Test with DN100 Blowdown Pipe in the PPOOLEX Facility," Research report poollex 2/2006, Lappeenranta University of Technology (2014).
13. I. Gallego-Marcos et al., "Effective momentum induced by steam condensation in the oscillatory bubble regime," *Nuclear Engineering and Design*, **350**, pp. 259–274 (2019).
14. T. Pättikangas et al., "CFD simulations of direct contact condensation of horizontal vapor jets," *Proc. Proceedings of 18th International Topical Meeting on Nuclear Reactor Thermal Hydraulics (NURETH-18), Portland, OR, August 18-22*, (2019).
15. C. H. Song, S. Cho, and H. S. Kang, "Steam Jet Condensation in a Pool: from Fundamental Understanding to Engineering Scale Analysis.," *J. Heat Transfer*, **134(3)**, pp. 031004.1–031004.15 (2012).
16. E. Hujala, V. Tanskanen, G. Patel, and J. Hyvärinen, "Image Analysis of Bubbling Mode Condensation Oscillations in Horizontal Sparger," *Proc. The 18th International Topical Meeting on Nuclear Thermal Hydraulics (NURETH-18), Portland, OR, August 18-August 23*, pp. 12 (2019).
17. E. Hujala, V. Tanskanen, and J. Hyvärinen, "Pattern recognition algorithm for analysis of chugging direct contact condensation," *Nuclear Engineering and Design*, **332**, pp. 202–212 (2018).
18. E. Hujala, *Quantification of large steam bubble oscillations and chugging using image analysis*, Acta Universitatis Lappeenrantaensis 871, Lappeenranta-Lahti University of Technology LUT, 2019, ISBN 978-952-335-424-1, ISBN 978-952-335-425-8 (PDF), ISSN 1456-4491, ISSN-L 1456-4491.
19. G. Patel, E. Hujala, M. Puustinen, and J. Hyvärinen, "Modeling of horizontal steam injection in a water pool," *Proc. The 19th International Topical Meeting on Nuclear Reactor Thermal Hydraulics (NURETH-19), Brussels, Belgium, March 6-March 11*, pp. 15 (2022).
20. D. Bestion and A. Guelfi, "Status and perspective of two phase flow modelling in the NEPTUNE multiscale thermalhydraulic platform for nuclear reactor simulation," *Nuclear Engineering and Technology*, **37/6**, pp. 511–524 (2005).
21. A. Guelfi et al., "NEPTUNE: A New Software Platform for Advanced Nuclear Thermal Hydraulics," *Nuclear Science and Engineering*, **156**, pp. 281–324 (2007).
22. J. Laviéville, E. Quémérais, S. Mimouni, M. Boucker, and N. Méchitoua, "NEPTUNE CFD V1.0 theory manual," EDF (2006).
23. L. Schiller and A. Naumann, "Über die grundlegenden berechnungen bei der schwerkraftbereitung," *Z. Vereins deutscher Ing.*, **77**, pp. 318–320 (1933).
24. L. Rayleigh, "Investigation of the character of the equilibrium of an incompressible heavy fluid of variable density," *Proc. London Math. Soc.*, **14**, pp. 170–177 (1883).
25. G. Taylor, "The instability of liquid surfaces when accelerated in a direction perpendicular to their planes Part I," *Proc. R. Soc. London, Ser., A* **201**, pp. 192–196 (1950).
26. S. Chen, F. Gerner, and C. Tien, "General film condensation correlations," *Exp. Heat Transfer*, **1**, pp. 93–107 (1987).
27. NIST Chemistry WebBook, "NIST Standard Reference Database Number 69," 2019.